Exp Fluids
DOI 10.1007/s00348-008-0468-6

RESEARCH ARTICLE

The laminar hole pressure for Newtonian fluids

Vasileios Symeonidis · Bruce Caswell

Received: 22 February 2007 / Revised: 16 January 2008 / Accepted: 23 January 2008

Abstract For flows with wall turbulence the hole pressure, P_H, was shown empirically by Franklin and Wallace (J Fluid Mech, 42, 33–48, 1970) to depend solely on R_+, the Reynolds number constructed from the friction velocity and the hole diameter b. Here this dependence is extended to the laminar regime by numerical simulation of a Newtonian fluid flowing in a plane channel (gap H) with a deep tap hole on one wall. Calculated hole pressures are in good agreement with experimental values, and for two hole sizes are well represented by: $(P_H - P_{HS})/\tau_w = \sqrt{(k^2 + c^2 R_+^2)} - k$, where the Stokes hole pressure $P_{HS}/\tau_w = s\,(b/H)^3$, k, c, s are fitted constants, and τ_w is the wall shear stress.

1 Introduction

The hole pressure or static pressure error, P_H, is the change of the normal wall traction resulting from the presence of a pressure tap on the wall of a channel as depicted in Fig. 1. P_H is the error incurred when the hydrostatic pressure deep within the hole is taken to be the *wall-pressure*. Pressure taps are widely used in turbulent flow, and for wall turbulence Franklin and Wallace (1970) found that for a wide range of hole sizes measured values of P_H, normalized by the wall stress τ_w, plotted as a single function of R_+, the Reynolds number constructed from the friction velocity and the hole diameter, b. The current interest in microchannels provides the motivation for the laminar flow case investigated numerically here. In this work negative normal wall tractions will be referred to as wall pressures. The hole pressure, P_H, is defined as the difference between pressure P_1 at the wall for the *undisturbed* channel flow and the static pressure P_2 at the bottom of the tap hole for the *disturbed* flow,

$$P_H = P_1 - P_2. \tag{1}$$

In most applications, the hole size relative to the channel dimension, wall curvature, or other geometric lengths are assumed to have a negligible effect on the hole pressure. For the plane channel this assumption was investigated by means of flow calculations for two hole sizes, and a substantial size effect was found for relative hole size $b/H = 1$ used in some experimental work (Lodge and Vargas 1983; Tong 1980). Although these studies were directed at the corresponding problem for non-Newtonian fluids, data were also measured for Newtonian fluids, and these are compared below with calculated values. This paper deals only with Newtonian fluids in laminar flow. The calculated results reported below demonstrate that pressure taps give rise to two global effects, namely:

1. The manometric error, or hole pressure P_H, due to the flow disturbance caused by the hole.
2. The recovered pressure, P_D, in the channel which measures the wall shear-stress relief, or reduced dissipation, due to the hole. Each hole shifts the linear Poiseuille pressure distribution upward by P_D, and hence it is a small systematic error incurred when two well-separated holes are used to measure the pressure loss in the undisturbed flow.

The clearest way to understand the intrusiveness of pressure taps is examination of the calculated disturbance

V. Symeonidis
Division of Applied Mathematics, Brown University,
Providence, RI 02912, USA

B. Caswell (✉)
Division of Engineering, Brown University,
Providence, RI 02912, USA
e-mail: caswell@dam.brown.edu; caswell@cfm.brown.edu

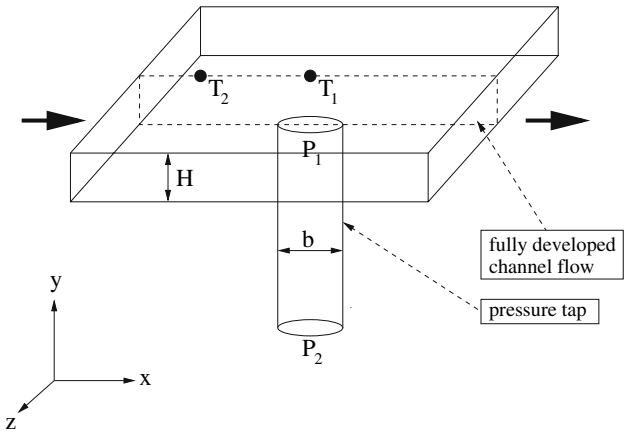

Fig. 1 Plane channel (gap H) with pressure tap (diam. b). T_1, T_2 are locations of pressure transducers in the stressmeter of Lodge and Vargas (1983), T_1 measures P_1 (Eq. 1) only for small b/H. A transducer at the bottom of the tap hole measures P_2

pressure field. Less insight is revealed from the disturbance velocity field. The undisturbed pressure field consists of the linear Poiseuille field in the channel and a uniform constant pressure in the hole; this constant is chosen to be the Poiseuille value at the streamwise position of the hole axis in Fig. 1. The undisturbed field can be considered an initial condition in which the two regions are isolated by a membrane placed across the mouth of the hole. At time zero, the membrane is removed and the flow evolves toward a new steady state. The disturbance pressure field is then the *difference* between the new steady state pressure field and the initial or undisturbed one. Unless otherwise noted the disturbance pressure will be referred to simply as the "pressure" In Stokes flow, the plane normal to the flow direction, coincident with the axis of the hole, is a plane of fore-aft symmetry for the streamlines, and anti-symmetry for the isobars. It follows that in the limit of small hole-Reynolds number the hole pressure P_H approaches one-half the pressure recovery P_D in the channel (see Fig. 3). This provides a consistency check for the calculations. As will be seen below, an unforeseen result of these calculations is that while P_H is a strong function of Re the recovered pressure, P_D, persists at its Stokes value well beyond the low Re Stokes regime where the fore-aft symmetry of the streamlines no longer holds.

For deep holes dimensional analysis of the problem depicted in Fig. 1 gives the dimensionless hole pressure as a function of the the relative hole size and a Reynolds number :

$$P_H/\tau_w = f(Re, b/H),$$
$$P_{HS}/\tau_w = f(0, b/H) \approx 0.032(b/H)^3, \qquad (2)$$

where P_{HS} is the Stokes flow value of P_H. Its approximate dependence on b/H was deduced from the simulations of

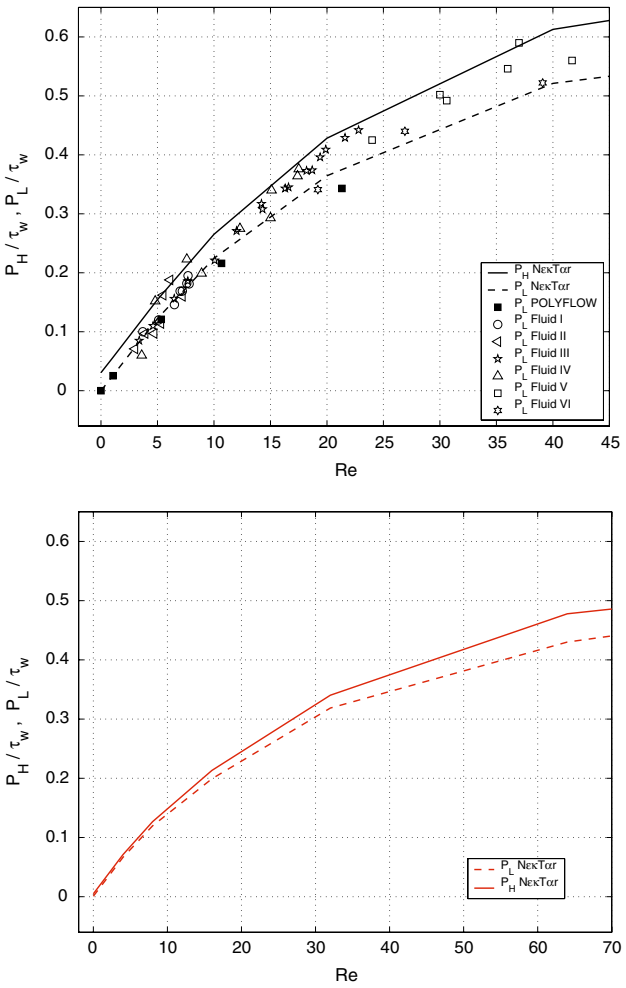

Fig. 2 Hole pressure versus Re for b/H = 1 (*upper*), and 1/2 (*lower*). Open points are Tong's (1980) P_L(see Fig. 1) measurements for various Newtonian fluids; calculated P_L values are: dashed curves by $\mathcal{N}\varepsilon\kappa\mathcal{T}\alpha r$, and *filled squares* by POLYFLOW. *Solid curves* are P_H (manometric error, Eq. 1) calculated by $\mathcal{N}\varepsilon\kappa\mathcal{T}\alpha r$

Symeonidis and Caswell (2007) for three hole sizes, and hence in the abstract formula the constant s is 0.032. Hole Reynolds numbers have been defined by Lodge and Vargas (1983) and by Franklin and Wallace (1970) respectively as:

$$Re = \dot{\gamma}_w bH/(4\nu), \quad R_+ = u_+ b/\nu = 2\sqrt{(Re\ b/H)} \qquad (3)$$

where $\dot{\gamma}_w, \tau_w = \mu\dot{\gamma}_w$ and $u_+ = \sqrt{(\tau_w/\rho)}$ are wall values of the shear rate, the shear stress and the friction velocity respectively for the undisturbed channel flow. The fluid properties are respectively: the shear viscosity μ, kinematic viscosity ν and density ρ. The simple relationship between these hole Reynolds numbers is a consequence of laminar channel flow. The hole is deep enough to ensure stagnant conditions for all channel flow rates of this study, and hence its depth is not a relevant parameter. Shallow holes have been investigated experimentally by James and Chandler (1993) with b/H = 0.7 and depths from 0 to

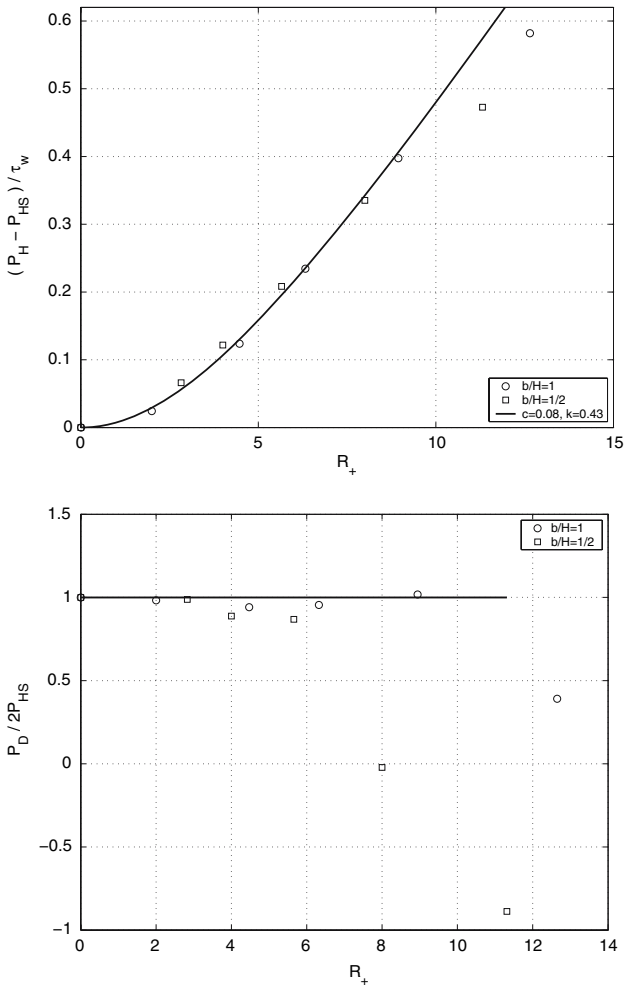

Fig. 3 Relative hole pressure (*upper*), $(P_H - P_{HS})/\tau_w$, and (*lower*) normalized recovered pressure (see Fig. 3) , $P_D/(2P_{HS})$ versus friction Reynolds number for $b/H = 1/2$ and 1. Open points calculated by $\mathcal{N}\varepsilon\kappa\mathcal{T}\alpha r$. Solid curve (*upper*): the fitted abstract formula

$0.63b$. For their greatest depth their measured hole pressures plotted against Reynolds number lie about about 10–20% above the deep hole data of Tong (1980) which indicates that a hole as shallow as $0.63b$ is close to being 'deep'. The hole depths of this study were $5.75b$ and $2.375b$ for $b/H = 1/2$, 1 respectively, while in the simulation of Crochet et al. (1986)the depth was $2b$.

Defined by (Eq. 1) the hole pressure is positive for all Reynolds numbers. Since they vanish as the relative hole size $b/H \to 0$, either of the *hole Reynolds numbers* defined in (Eq. 3) is an appropriate measure of inertial effects due to the hole. Hence R_+ can be substituted for Re in (Eq. 2). Since the channel flow is specified to be in the laminar regime the channel Reynolds number, $Re(H/b)$, is not a relevant parameter. For non-Newtonian fluids the hole pressure effect at low Reynolds number is dominated by the first normal-stress difference which yields a negative P_H, and for this reason Lodge and Vargas (1983) defined P_H to be the negative of (Eq. 1). They also assumed that P_1 can be measured as the wall pressure on the wall opposite the hole , T_1 in Fig. 1. The accuracy of this assumption for Newtonian fluids is investigated in this work. The hole pressure calculated from the Lodge location for P_1 will hereafter be denoted by P_L. The relation between P_H and P_L can be determined from either very exacting measurements or from a solution of the Navier–Stokes equation. In view of the geometry the latter implies numerical simulation.

2 Numerical method

For the discussion of the numerical simulations it is convenient to render the Navier–Stokes equation dimensionless with the channel parameters,

$$\frac{\partial \mathbf{u}}{\partial t} + Re(H/b)[\mathbf{u} \cdot \nabla \mathbf{u}] = -\nabla p + \nabla^2 \mathbf{u}, \tag{4}$$

where $\mathbf{u}$ denotes the velocity vector, p the scalar pressure, and Re (H/b) is the channel Reynolds number (see Eq. 3), which in all cases was set well below the known laminar-turbulent transition value. The solution is obtained by marching in time to the steady state from a known initial state, and hence the scale of the dimensionless time t is determined by the magnitude of the time step, δt. The numerical solution of (Eq. 4) was carried out with the $\mathcal{N}\varepsilon\kappa\mathcal{T}\alpha r$ code described in Karamanos et al. (1999). The *temporal discretization* employs the time-splitting, stiffly-stable scheme of Karniadakis et al. (1991), which enhances stability through backwards time-differencing. Time-splitting allows for the sequential solution of the pressure and the velocity components which are determined respectively by time-independent Poisson and Helmholtz operators. These properties of the scheme allow a large number of degrees of freedom to be handled economically. While higher order temporal accuracy can be specified, for the laminar flows of this work second order accuracy in δt suffices for convergence to a steady-state.

The *spatial discretization* follows the spectral/*hp* element method described in Karniadakis and Sherwin (1999) with standard unstructured and hybrid grids, and has been implemented in the two and three-dimensional serial and parallel versions of $\mathcal{N}\varepsilon\kappa\mathcal{T}\alpha r$, Karamanos et al. (1999). Jacobi polynomials with mixed weights are the hierarchical basis for these spectral elements which have N modes per direction. It can be demonstrated by comparison with analytical solutions that the spatial convergence of spectral elements is exponential in the mode number N. Solutions were monitored at selected points (including some near the aperture) as follows: 1. the tolerances for the iterative solver were set at 10^{-6} for the dimensionless velocity fields and 10^{-5} for the dimensionless total pressure field. 2. the

resulting disturbance pressure fields near the hole were compared for modal orders $N = 3$, 4 and $N = 6$, for each of $Re = 0$, 5, 20. By construction the disturbance pressure contains the pressure fluctuations associated with the time-marching iterations. Typically these fluctuations were largest near the aperture, and hence that region determined the run times required to achieve steady states within the tolerances. In the upstream channel where P_H was measured (see Fig. 6), and in other regions far from the hole, the fields attained their final values much sooner with fluctuations well below the tolerances. For the given mesh and within the tolerances, it was found that no significant improvement was realized between $N = 4$ and 6, and in view of the rapid overhead increase with N the simulations of this work were carried out with $N = 4$. The limitation to relatively low spectral order N is a reflection of the integrable singularity at the sharp edge of the aperture which would be expected for an exact solution of the Navier–Stokes system. For smooth boundaries higher spectral orders are generally attainable (see Ma et al. 2003; Symeonides and Caswell 2007). The dimensions of the channel were scaled to the half-gap $H/2$. In the main channel (gap = 2) the undisturbed Poiseuille flow was normalized with unit maximum velocity. The overall dimensionless pressure drop for the channel of length 19 is 38. Thus the P_H magnitudes given below between 0.01 and 0.7 are calculated with a loss of between two and three digits. The disturbance streamwise, cross-stream and transverse velocity components, respectively u, v and w, have relative magnitudes $u \approx 10v \approx 100w$ as can be seen in the contour plots which follow. Hence the simulation is challenged by many of the difficulties associated with the physical measurement of a second order effect.

In this work the meshes which describe the space of Fig. 1 were constructed with ample width to eliminate edge effects, and upstream end effects. Initially the borders of the mesh were chosen to be 10 by 10 planes with the hole in the center as in Crochet et al. (1986). After tests the mesh was improved by doubling the downstream length. The final mesh was further improved to a width of 12 and upstream and downstream lengths of 7 and 12 respectively. The upstream and width extensions resulted in almost imperceptible changes of the solution fields. To recover a level downstream disturbance pressure the required downstream length increases with Reynolds number, and this places an upper limit on that parameter for a given length (see Figs. 4 and 5 below). At $Re = 20$ and 40 the downstream length change from 5 to 12 increases P_L and P_H by about 3 and 4% respectively. Crochet et al. (1986) imposed symmetry on a half-space mesh defined on one side of the central plane. Downstream they imposed zero lateral velocities, and then used the downstream recovery of the main Poiseuille flow as their criterion for acceptance at the highest Re. In this work the recovery of Poiseuille flow was found to be an insensitive indicator compared to the disturbance pressure. The meshes are highly refined in the vicinity of the hole, and yield a nodal space of $O(10^6)$ degrees of freedom. The boundary conditions were set as follows: the Poiseuille velocity at the entry, outflow conditions, $\partial \mathbf{u}/\partial n = 0, p =$ constant at the exit, and periodic conditions on the edge planes.

3 Numerical results for circular holes

Hole pressure vs. Reynolds number (Eq. 3a) are plotted in Fig. 2 for hole sizes; $b/H = 1$ and $b/H = 1/2$. While the former appears to be unusually large it was chosen to correspond to the experiments of Tong (1980) whose data are displayed as open points. Two curves calculated by $\mathcal{N}\varepsilon\kappa\mathcal{T}\alpha r$ are shown in each plot. The solid and the dashed lines representing P_H and P_L respectively. For the former P_1 in (Eq. 1) was taken to be the undisturbed, Poiseuille wall pressure at the hole axis, and for the latter it was taken to be the wall pressure *for the disturbed flow* at the point of intersection of the hole axis with the opposite wall. By symmetry P_L is identically zero in the Stokes regime, but P_H, denoted as P_{HS}, was found to vanish as $(b/H)^3$ by Symeonidis and Caswell (2007), see (Eq. 2b). For $b/H = 1/2$ the second plot shows that while P_H and P_L are initially almost equal their difference grows and becomes measurable as Re increases. For $Re < 10$ Tong's measured values are in very good agreement with the calculated P_L curves of this work and with the earlier work of Crochet et al. (1986) who calculated P_L (filled squares) with the POLYFLOW code. However, as Re increases the data show increased scatter and generally lie above the calculated values. This may be due to the many problems described by Tong (1980) with the calibration of flush-mounted pressure transducers. As Re increases the POLYFLOW results trend below the P_L curve calculated by $\mathcal{N}\varepsilon\kappa\mathcal{T}\alpha r$, and this appears to be due to insufficiency of downstream length, and the coarseness of their mesh.

The upper graph of Fig. 3 shows that, for both $b/H = 1$, and 1/2, $(P_H - P_{HS})/\tau_w$, the calculated hole pressure relative to its Stokes value, plots very closely as a function of the single variable R_+ (see Eq. 3b). The corresponding P_L values for $b/H = 1/2$ and 1 do not correlate very well compared to the correlation of Fig. 3. Additional simulations are required to know whether the correlation of Fig. 3 holds for $b/H > 1$. Of course, for very large b/H the concept of a disturbed channel flow loses its meaning. For turbulent boundary layers generated in a wind-tunnel Franklin and Wallace (1970) found that measured values of P_H were well-correlated as a function of R_+ alone for a

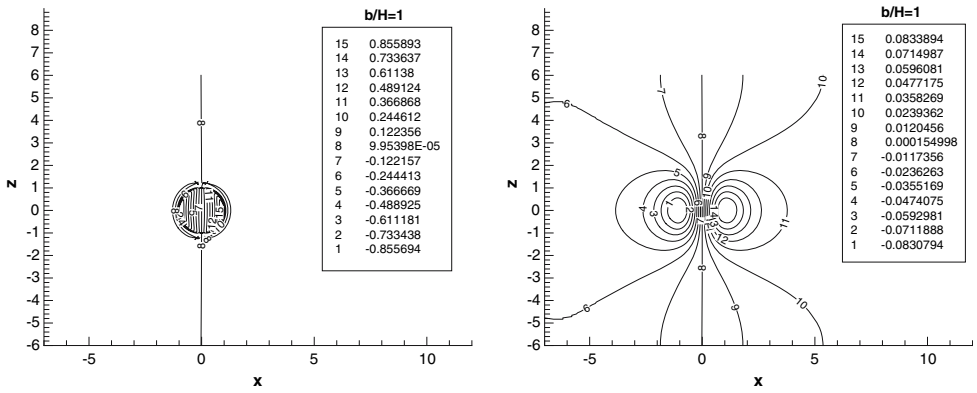

Fig. 4 Pressure distributions on lower ($\{x, -1, z\}$, *left*) and upper ($\{x, 1, z\}$, *right*) walls; $Re = 0$, $b/H = 1$. Positive contours lie to the right of $x = 0$

wide range of hole sizes. Clearly, in turbulent flow P_{HS} is negligible, and indeed it is measurable in laminar flow only for $b/H \sim O(1)$. Although the fitted curve of the Franklin and Wallace (1970) correlation has a similar approach to the origin as in Fig. 3, the smallest R_+ of their data lie well beyond the largest value of this work. Moreover, none of their data is identified to be in the laminar regime, nor does their turbulent boundary layer flow correspond to the fully developed, laminar channel flow of Fig. 1. The solid curve was computed from the two-parameter, empirical formula of the abstract with $k = 0.43$, $c = 0.08$; this fit represents the numerical values of P_H with good accuracy up to Re of 25 in Fig. 2. As $R_+ \to 0$ this formula has the expansion

$$(P_H - P_{HS})/\tau_w \approx c^2 {R_+}^2/(2k) = 0.030 Re(b/H) + O({R_+}^4) \quad (5)$$

where the numerical coefficient was calculated from the fitted values of k, c. For P_L, the dashed curve of Fig. 2 (top) departs from the origin with a slope of 0.024, which confirms the value derived by Lodge and Vargas (1983) from Tong's (1980) data up to $Re = 10$ and was previously confirmed by the Crochet et al. (1986) simulation.

The recovered pressure P_D, normalized by 2 P_{HS}, is displayed in the lower graph of Fig. 3. In Stokes flow this ratio is unity by the anti-symmetry of the pressure field, and yet it persists at this value as R_+ increases into the range where P_H itself is strongly variable. No theoretical argument can be given for this result. This is remarkable because of the limited numerical accuracy of the normalization factor, P_{HS}, which by (Eq. 2) is about an order of magnitude smaller at $b/H = 1/2$ than at $b/H = 1$. Once the ratio departs from unity the calculated ratios no longer plot as functions of the single variable R_+. This may be an indication that full recovery of the Poiseuille velocity and pressure fields were not achieved at the highest Re.

For $b/H = 1$ calculated pressures, normalized by τ_w, are plotted as contours on the upper and lower channel walls (x, ± 1, z) in Figs. 4 and 5 at Re $b/H = 0$, and 20 respectively. These contours show that the disturbance pressure traverses the channel gap and the channel width with little attenuation. The peaks in the vicinity of the hole are smoothed out, but the ramp-like increase of $O(P_D)$ is projected across the gap and laterally across the full width of the channel. In Fig. 4 for $Re(b/H) = 20$, or $R_+ = 9$ the pressure wake is captured on the upper plane, and further increase in the Reynolds number will extend it to the exit plane. The lower plane contours are highly concentrated near the lip, reflecting the singular behavior expected for the sharp-edged holes. In Figs. 4 and 5 the smoothness and symmetry of the contours with respect to the center plane $z = 0$ implies that steady laminar flow was achieved. The second order magnitude of the disturbance pressure in the

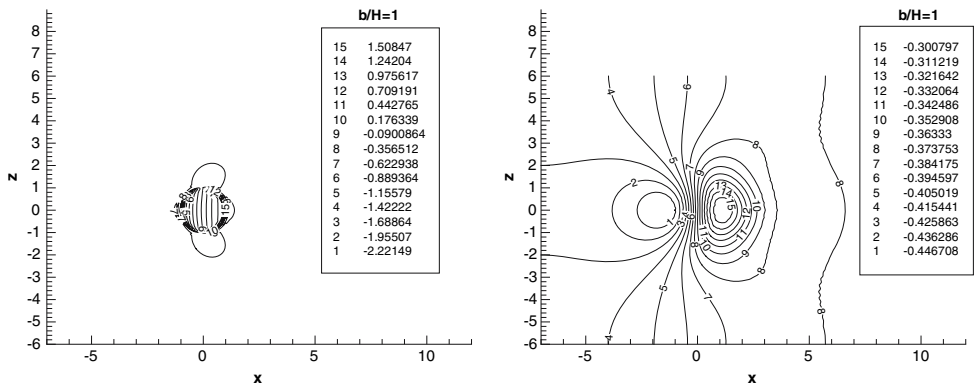

Fig. 5 Pressure distributions on lower ($\{x, -1, z\}$, *left*) and upper ($\{x,1,z\}$, *right*) walls; $b/H = 1$, $Re = 20$, $R_+ = 9$

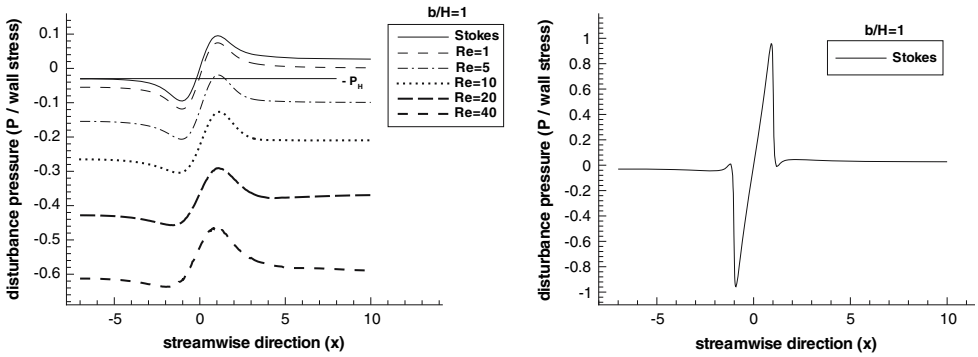

Fig. 6 Streamwise pressure profiles in center plane on the upper ($\{x, 1, 0\}$, *left*) and lower ($\{x, -1, 0\}$, *right*) walls, $b/H = 1$. Pressure constant set to give $P_2 = 0$ in Fig. 1. P_D = right-left asymptote

channel (see Sect. 2 above) reinforces this conclusion. Accuracy limitations (see Sect. 2 above) prevent the wake signature in the velocity field to be distinguished from numerical error. As Re increases to a point beyond the range reported here the hole may induce unsteady and unsymmetric disturbances.

Figure 6 shows the centerline ($z = 0$ in Figs. 4 and 5) pressure profile on the lower, and upper wall of the channel for $b/H = 1$. The pressure constant is chosen so that the pressure is zero at $(0, -d, 0)$, the center of the bottom plate of the hole at depth d. By this definition the far upstream ($x = -7$) value of the pressure on the upper plate is the negative of P_H as indicated in Fig. 3, and the difference between the far downstream ($x = 12$) and far upstream ($x = -7$) values is the recovered pressure P_D due to reduced dissipation relative to the no-hole geometry. At the intersection of the hole axis $x = 0$ and the upper plate the pressure is P_L. If P_H is added to each curve then the pressure will be zero, i.e. undisturbed, far upstream, P_H at the bottom of the hole, and P_D far downstream. The advantage of setting the pressure to zero at the hole bottom is that P_H, P_L and P_D can be conveniently displayed on one plot. On the plane opposite the hole the main effect of inertia is to shift the profiles vertically with little change in shape which may account for the tendency of $P_D/(2P_{HS})$ in Fig. 3 to remain at its Stokes value. As the pressure wake develops at $Re(b/H)$ of about 20 the centerline disturbance pressure does not quite level off at the exit plane as required for the full recovery of the Poiseuille gradient, and this accounts for the departure of $P_D/(2P_{HS})$ from unity at the higher Reynolds numbers in Fig. 3. Runs at Re greater than those of Fig. 3 showed further steepening of the exit profiles.

Centerplane streamlines and contours of the u velocity component at the aperture $(x, -1, z)$ for $Re(b/H) = 32$ or $R_+ = 11$ are shown in Fig. 7; the fore-aft asymmetry is typical of inertial effects. In Stokes flow these streamlines have fore-aft symmetry, and the u-contours are concentric circles. Symmetry about the central plane $z = 0$ is not imposed directly, and small numerical errors in the velocity field give rise to small asymmetries which accumulate in the pathline calculation as manifested in the spurious ending of the weak recirculation near the bottom of the hole. This secondary flow is very much weaker than the upper one, and gives rise to a negligible pressure over the hydrostatic value at the bottom. Aperture contours of the v and the w components are displayed in Fig. 8 In Stokes flow the v-contours are anti-symmetric about the plane $x = 0$ and the w-contours have four-fold anti-symmetry with respect to the planes $x = 0$ and $z = 0$.

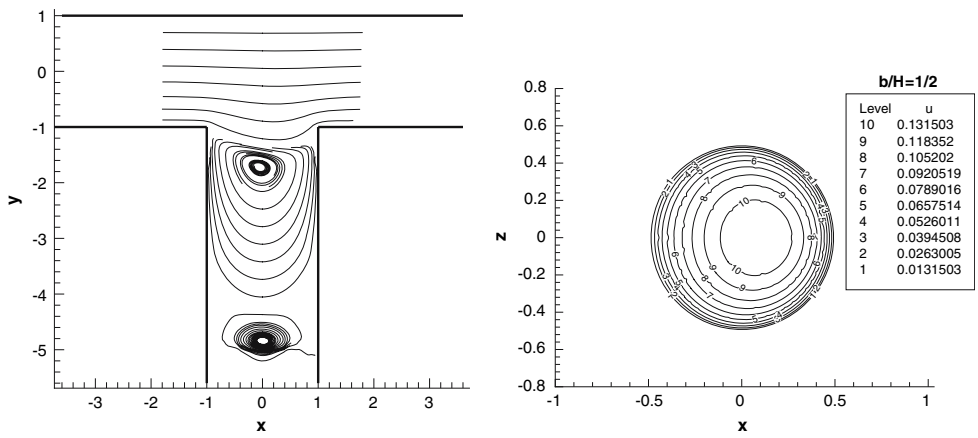

Fig. 7 Centerplane, $\{x, y, 0\}$, streamlines for $b/H = 1$ at $Re = 20$ or $R_+ = 9$ (*left*), and u-velocity contours at the lower-wall aperture for $b/H = 1/2$ at $Re = 64$, $R_+ = 11$ (*right*)

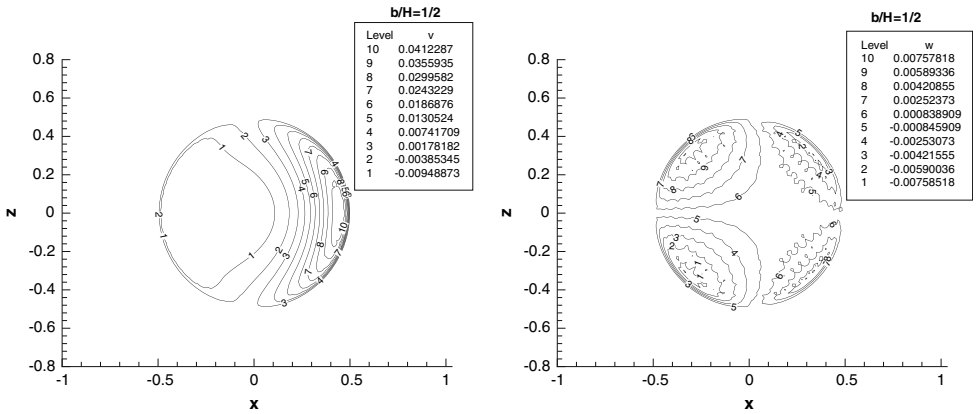

Fig. 8 Contours of the *v*-velocity (*left*) and the *w*-velocity (*right*) at the lower-wall aperture for $b/H = 1/2$ at $Re = 64$, $R_+ = 11$

4 Conclusions

Numerical calculations of the laminar flow of a Newtonian fluid in a channel with a deep-hole pressure tap on one wall have yielded a correlation for the relative hole pressure $P_H - P_{HS}$ as a function of the friction Reynolds number, Re_+ alone. The limiting Stokes value P_{HS} being a function of hole size b/H alone implies that the general function of two variables derived from dimensional analysis (Eq. 2) is the sum of two functions of one variable. Since P_{HS} is negligible for holes less than $O(1)$, the functionality of the correlation for P_H is essentially the same as that known for turbulent boundary layers. The hole pressure is well represented by the formula given in the abstract up to R_+ of about 10. The recovered pressure was shown to remain at twice the Stokes value up to about the same value of R_+. Similarity with respect to hole size allows experimental designs to be explored for all sizes up to $b/H \sim O(1)$.

Acknowledgments This work was supported by NSF (grant number CTS-0326702). The authors gratefully acknowledge the advice and guidance of George Em Karniadakis during the course of this work.

References

Crochet MJ, Dupont S, Marchal JM (1986) Numerical calculation of the Newtonian circular hole pressure. J Rheol 30(S):S91–S96

Franklin FE, Wallace JM (1970) Absolute measurements of static-hole error using flush transducers. J Fluid Mech 42:33–48

James DF, Chandler GM (1993) Measurements of hole pressure at various depths for Newtonian and non-Newtonian fluids. J Rheol 37:893–909

Karamanos G-S, Evangelinos C, Kirby RM, Karniadakis GE (1999) DNS of turbulence on a PC/Linux cluster: fact or fiction? Proc Supercomputing

Karniadakis GE, Sherwin SJ (1999) Spectral/*hp* element methods for CFD. Oxford University Press, Oxford

Karniadakis GE, Israeli M, Orszag SA (1991) High-order splitting methods for incompressible Navier–Stokes equations. J Comp Phys 97:414

Lodge AS, de Vargas L (1983) Positive hole pressures and negative exit pressures generated by molten polyethylene flowing through a slit die. Rheol Acta 22:151–170

Ma X, Symeonidis V, Karniadakis GE (2003) A spectral vanishing viscosity method for stabilizing viscoelastic flows. J Non-Newtonian Fluid Mech 115:125–155

Symeonidis V, Caswell B (2007) The limiting hole pressure in three dimensions. J Non-Newtonian Fluid Mech 145:57–68

Tong PP-L (1980) Fundamental studies on a laboratory stressmeter. PhD thesis, University of Wisconsin-Madison